

# A numerical benchmark test for continuous casting of steel

B Šarler<sup>1,3</sup>, R Vertnik<sup>1,2</sup> and K Mramor<sup>3</sup>

<sup>1</sup> Laboratory for Multiphase Processes, University of Nova Gorica, Vipavska 13, SI-5000 Nova Gorica, Slovenia

<sup>2</sup> Štore Steel d.o.o., Technical Development, Železarska 3, SI-3220 Štore, Slovenia

<sup>3</sup> COBIK Center of Excellence for Biosensorics, Automation and Process Control, Solkan, Slovenia

E-mail: bozidar.sarler@ung.si, robert.vertnik@store-steel.si,  
katarina.mramor@cobik.si

**Abstract.** There is a continuously developing need for benchmarking of solidification simulations - from the theoretical as well as from the applied points of view. The benchmarking is usually done in two parts. The verification part confirms the proper numerical solution (Are we solving the equations correctly?) and the validation part (Are we solving the right equations?) confirms the proper response of the simulations regarding the experimental evidence. The history of related benchmarking shows differences of the results between different numerical methods, and differences in comparison with the experiments when solving even quite simple solidification situations. The present benchmark test proposes the verification benchmark for continuous casting of steel. Since the simulations of the temperatures, velocities, pressures and concentrations in the continuous casting represent a multiscale and multiphysics problem of high complexity (far away from a closed form solution), the verification can be done only by comparing the results of different numerical methods for solving the same governing equations. This has been done in the context of continuous casting by breaking the considered two dimensional problem into several sub problems by increasing complexity of geometry (straight in vertical direction, curved), boundary conditions (linear, non-linear), material properties (only Fe and Fe - C), microscopic considerations (Lever rule and Scheil rule). The governing equations complexity first involves only convective - diffusive heat transport with a predetermined velocity field, and assumed laminar and turbulent velocity calculations afterwards, modelled by a low Reynolds number turbulence model. Further complications involve the presence of the electromagnetic forces. The paper represents guidelines for the presentation of the numerical method, discretisation and results, as well as some of the results, obtained by the commercial finite volume based code and our in-house meshless method based laboratory code.

## 1. Introduction

Continuous casting [1] is the most common process in the production of steel. The process starts by pouring the molten metal into to the water cooled mould, where cooling intensity is high enough to solidify steel around the inner surface of the mould and generates the solid shell with molten metal in the centre of strand. After several minutes, the strand is pulled into the secondary cooling system,

which contains water spray systems with much smaller cooling intensity as in the water channels in the mould, and rollers, which support and guide the strand up to the end of the casting machine. The quality of the casted product (round or square billets, blooms or slabs) depends mainly on the process parameters in the mould region, where complex physical phenomena occur. The liquid metal, poured with a high velocity from the submerged entry nozzle (SEM) into the mould, produces turbulent flow with several re-circulating zones. Large heat fluxes, extracted from the mould, are a consequence of very high flow rates of the cooling water in the mould channels. It is impossible to measure temperature and velocity field inside the strand due to the very high temperatures of steel and inaccessibility of the region during the process. The numerical models [2] help us to better understand the casting behaviour and to further improve and optimize the process, particularly in such experimentally sophisticated situations. Various numerical methods have already been used to simulate the described problem, such as Finite Volume Method (FVM) [3-7], Finite Element Method (FEM) [8], and more advanced meshless method, like the Local Radial Basis Function Collocation Method (LRBFCM) [9-11]. Only very recently, different computational models (different governing equations, combined with different numerical methods) have been compared to assess the typical flow situations in continuous casting process [12] and their relation to model experiments. The solidification simulations are usually tested on a sequence of benchmarks that follow NAFEMS-type heat conduction simulations [13], convective diffusive cases with phase change [14], natural convection cases [15], solid-liquid specific cases with freezing of pure substance [16,17] and solidification of binary alloy [18,19]. However, until now, there is a lack of benchmark tests that would enable verification of numerical methods for solving transport phenomena in continuous casting of steel in an ordered way. There are no systematic well documented benchmark tests currently existing even for such a simple continuous casting models like the slice model [20]. In this paper, a simple benchmark test for the numerical solution of the continuous casting of steel is proposed. The main aim of the test is to compare the results of different numerical methods of the same physical model.

The presented physical model considers turbulent fluid flow with electromagnetic forces, solidification, and macrosegregation. The solution procedure is based on explicit time discretization and fractional step method [21] for velocity-pressure coupling. Turbulent flow is modelled by the two-equation eddy-viscosity model with the low-Re corrections. The numerical results are shown for the case without electromagnetic forces and macrosegregation, and with simplified microsegregation model. The meshless LRBFCM is used for the spatial discretization. The comparison is made with the results obtained by the commercial software Fluent, which is based on the FVM. The objective of this exercise is to test the ability of different numerical methods and algorithms to agree on a solution and to produce a reference numerical solution of the given problem.

## 2. Governing equations

The system of equations, describing the heat and fluid flow with solidification in the continuous casting of steel, is derived based on the mixture continuum formulation by Bennion and Incropera [22] and Reynolds time-averaging approach for modelling incompressible turbulent flow [23]. The time-averaged transport equations for mass, energy, momentum and solute conservation are

$$\nabla \cdot \mathbf{u} = 0, \quad (1)$$

$$\rho \frac{\partial \mathbf{u}}{\partial t} + \rho \nabla \cdot (\mathbf{u} \mathbf{u}) = -\nabla P + \nabla \cdot [2(\mu + \mu_t) \mathbf{S}] - \frac{2}{3} \rho \nabla k - \mu_L \frac{K_0 (1 - f_L^2)}{f_L^3} (\mathbf{u} - \mathbf{u}_s) + \mathbf{F}_b + \mathbf{F}_m, \quad (2)$$

$$\rho \frac{\partial h}{\partial t} + \rho \nabla \cdot (\mathbf{u} h) = \nabla \cdot (\lambda \nabla T) + \rho \nabla \cdot [f_s (h_L - h_s) (\mathbf{u} - \mathbf{u}_s)] + \nabla \cdot \left( f_L \frac{\mu_t}{\sigma_T} \nabla h_L \right), \quad (3)$$

$$\rho \frac{\partial C}{\partial t} + \rho \nabla \cdot (\mathbf{u} C) = \nabla \cdot (f_s D_s \nabla C_s + f_L D_L \nabla C_L) + \rho \nabla \cdot [(\mathbf{u} - \mathbf{u}_s)(C_L - C)] + \nabla \cdot \left( \frac{f_L \cdot \mu_t}{\sigma_c} \nabla C_L \right) \quad (4)$$

with  $\mathbf{u}$ ,  $P$ ,  $h$ ,  $T$  and  $C$  for velocity, pressure, enthalpy, temperature and solute concentration, respectively, and  $\rho$ ,  $\mu$ ,  $\mu_t$ ,  $f$ ,  $\lambda$ ,  $D$  are standing for density, molecular dynamic viscosity, turbulent dynamic viscosity, volume phase fraction, thermal conductivity, and diffusivity of the material. In above equations, subscripts  $L$  and  $S$  denote liquid and solid phase.  $\mathbf{S}$  stands for the strain-rate tensor. The fourth term in equation (2) represents the Darcy term, where  $K_0$  is the morphology constant of the porous medium and  $\mathbf{u}_s$  is velocity of the solid phase. The fifth term in equation (2) represents the buoyancy forces, defined as

$$\mathbf{F}_b = \rho [\beta_T \mathbf{g}(T - T_{ref}) + \beta_C \mathbf{g}(C_L - C_{ref})] \quad (5)$$

where  $\beta_T$ ,  $\beta_C$ ,  $T_{ref}$  and  $C_{ref}$  stand for thermal expansion coefficient, solute expansion coefficient, reference temperature and reference concentration, respectively. The turbulent dynamic viscosity is defined as

$$\mu_t = \rho c_\mu f_\mu \frac{k^2}{\varepsilon} \quad (6)$$

where  $k$  and  $\varepsilon$  are kinetic energy and dissipation rate, respectively. They are calculated by the following transport equations

$$\rho \frac{\partial k}{\partial t} + \rho \nabla \cdot (\mathbf{u} k) = \nabla \cdot \left[ \left( \mu_L + \frac{\mu_t}{\sigma_k} \right) \nabla k \right] + P_k - \rho \varepsilon + \rho D + \mu_L \frac{K_0 (1 - f_L^2)}{f_L^3} k, \quad (7)$$

$$\rho \frac{\partial \varepsilon}{\partial t} + \rho \nabla \cdot (\mathbf{u} \varepsilon) = \nabla \cdot \left[ \left( \mu_L + \frac{\mu_t}{\sigma_\varepsilon} \right) \nabla \varepsilon \right] + \rho (c_{1\varepsilon} f_1 - c_{2\varepsilon} f_2 \varepsilon) \frac{\varepsilon}{k} + \rho E + \mu_L \frac{K_0 (1 - f_L^2)}{f_L^3} \varepsilon. \quad (8)$$

In equations (3,4,6-8)  $c_\mu$ ,  $f_\mu$ ,  $c_{1\varepsilon}$ ,  $f_1$ ,  $c_{2\varepsilon}$ ,  $f_2$ ,  $\sigma_T$ ,  $\sigma_C$ ,  $\sigma_k$  and  $\sigma_\varepsilon$  are the closure coefficients, while  $D$  and  $E$  are additional source terms of the low-Reynolds turbulent model [23].

The last term on the left side of equation (2) represents the electromagnetic force acting on the conductive material moving through the induced magnetic field, defined as

$$\mathbf{F}_m = \mathbf{J} \times \mathbf{B} \quad (9)$$

where  $\mathbf{J}$  and  $\mathbf{B}$  are the induced current density and the magnetic flux density. The current density is calculated by Maxwell equations [5,6] under assumption that the induced magnetic field is negligible in comparison with external applied magnetic field

$$\nabla \cdot \mathbf{J} = 0, \quad (10)$$

$$\mathbf{J} = \sigma (\mathbf{E} + \mathbf{u} \times \mathbf{B}), \quad (11)$$

$$\mathbf{E} = -\nabla \phi \quad (12)$$

where  $\sigma$  is electrical conductivity,  $\mathbf{E}$  is electric field density and  $\phi$  is electrical potential, calculated from the following equation

$$\nabla^2 \phi = \nabla \cdot (\mathbf{u} \times \mathbf{B}). \quad (13)$$

The constitutive temperature-enthalpy relationship  $h_s$  and  $h_L$  in equation (3) are defined as

$$h_s = \int_{T_{ref}}^T c_{ps} dT, \quad (14)$$

$$h_L = \int_{T_{ref}}^{T_s} c_{ps} dT + \int_{T_s}^T c_{pL} dT + h_m = h_s(T) + \int_{T_s}^T (c_{pL} - c_{ps}) dT + h_m, \quad (15)$$

respectively. The liquid fraction  $f_L$ , concentration of solute in liquid phase  $C_L$ , partition ratio  $k_p$ , and liquidus temperature  $T_L$  are determined based on the level rule microsegregation model, i.e.

$$f_L = 1 - \frac{1}{1-k_p} \frac{T-T_L}{T-T_m}, \quad C_L = \frac{C}{1+f_s(k_p-1)}, \quad k_p = \frac{C_s}{C_L}, \quad T_L = T_m + (T_e - T_m) \frac{C}{C_e} \quad (16,17,18,19)$$

where  $T_m$ ,  $T_e$  and  $C_e$  are melting temperature, eutectic temperature and solute concentration in eutectic alloy, respectively. They are obtained from the phase diagram for the iron-carbon system.

### 3. Solution procedure

Our solution procedure is based on the novel meshless technique that follows the following steps. We seek the solution of the equations for the velocity, pressure, temperature, concentration, turbulent kinetic energy, dissipation and current density at time  $t+t_0$  by assuming known fields  $\mathbf{u}$ ,  $p$ ,  $T$ ,  $C$ ,  $k$ ,  $\varepsilon$  and  $\mathbf{J}$  at time  $t_0$  and known boundary conditions at time  $t > t_0$ . The coupled set of mass conservation equation (1) and momentum conservation equations (2) are solved by the fractional step method [21], where the continuity of the mass (1) is considered by constructing the pressure Poisson's equation. The governing equations are discretized by using the explicit time discretization. This leads to the following algorithm, summarized through the following 8 steps:

1) The intermediate velocity components are calculated without the pressure gradient

$$\mathbf{u}^* = \mathbf{u}^n + \frac{\Delta t}{\rho} \left[ -\rho \nabla \cdot (\mathbf{u} \mathbf{u}) + \nabla \cdot [2(\mu + \mu_t) \mathbf{S}] - \frac{2}{3} \rho \nabla k - \mu_L \frac{K_0 (1-f_L^2)}{f_L^3} (\mathbf{u} - \mathbf{u}_s) + \mathbf{F}_b + \mathbf{F}_m \right]^n. \quad (20)$$

2) The pressure Poisson equation is treated

$$\nabla^2 P^{n+1} = \frac{\rho}{\Delta t} \nabla \cdot \mathbf{u}^* \quad (21)$$

by solving the related sparse matrix [11].

3) The velocity components are corrected by the pressure gradient

$$\mathbf{u}^{n+1} = \mathbf{u}^* - \frac{\Delta t}{\rho} \cdot \nabla P^{n+1}. \quad (22)$$

4) After the solution of the velocity field, the transport equations for energy is solved

$$h^{n+1} = h^n + \frac{\Delta t}{\rho} \left[ -\rho \nabla \cdot (\mathbf{u} h) + \nabla \cdot (\lambda \nabla T) + \rho \nabla \cdot [f_s (h_L - h_s) (\mathbf{u} - \mathbf{u}_s)] + \nabla \cdot \left( f_L \frac{\mu_t}{\sigma_t} \nabla h_L \right) \right]^n. \quad (23)$$

5) The temperature field is calculated from the enthalpy field, calculated in previous step, using the inverse of the constitutive temperature-enthalpy relationships (14,15), i.e.  $T = T(h)$ .

6) Species concentration, turbulent kinetic energy and dissipation rate fields are calculated. They are discretized by the same way as the transport equation (23).

- 7) The current density field is updated by the following procedure. First, the electrical potential is obtained by solving the Poisson equation (13). After that, the electric field intensity is calculated from the equation (12). Finally, the current density is obtained from the equation (11).
- 8) The turbulent viscosity (6), solute concentrations (17,18) and liquidus temperature (19), are updated for each node. The solution is set ready for the next time step.

All derivatives of the transport equations are calculated by the LRBFCM [9,11,13,24], where the collocation is made locally on overlapped sub-domains. On each sub-domain, the scalar function  $\Phi$  (standing for temperature, species concentration, velocity components, pressure, turbulent kinetic energy, turbulent dissipation rate, magnetic flux components, and current density components) is represented over a set of (in general) non-equally spaced nodes  $\mathbf{p}_n$ ;  $n = 1, 2, \dots, N$  in the following way

$$\Phi(\mathbf{p}) \approx \sum_{k=1}^K \psi_k(\mathbf{p}) \alpha_k, \quad \psi_k(\mathbf{p}) = [r_k^2 + c^2]^{1/2} \quad (24,25)$$

where  $\psi_k$  stands for the multi-quadric radial basis shape functions [25],  $\alpha_k$  for the coefficients of the shape functions, and  $K$  represents the number of the shape functions. In equation (25)  $c$  represents the shape parameter and  $r_k$  the radial distance between two points in the sub-domain. The detailed procedure of calculating the derivatives with the LRBFCM can be found in [11,13].

#### 4. Benchmark description

##### 4.1. Geometry

The proposed benchmark represents a simplified 2D model of the continuous casting process. The geometry of the simplified casting machine is shown in figure (1). A billet with a square cross-section is assumed. The computational domain represents half of the longitudinal section of the billet with length 1.8 m, shown in figure (2). These simplifications are used mainly for straightforward verification of the developed numerical model, and in order to reduce the CPU time of the simulations. The dimensions of the casting geometry are billet width  $a_b = 0.14\text{m}$ , diameter of the SEN  $d_2 = 0.035\text{m}$ , mould height  $l_m = 0.8\text{m}$  and height of the coils  $l_{EMS} = 0.1\text{m}$ , respectively.

##### 4.2. Material properties

Generally, the material properties of steel are temperature dependent. However, for benchmark purpose, constant but different values are used for each phase. They are given in table (1).

**Table 1.** Material properties.

$\rho$ (kg m <sup>-3</sup> )	$c_p$ (J kg <sup>-1</sup> K <sup>-1</sup> )	$\lambda$ (W m <sup>-2</sup> K <sup>-1</sup> )	$\mu$ (kg/m s)	$T_L$ (K)	$T_S$ (K)	$h_m$ (J/kg)	$K_0$ (m <sup>-2</sup> )	$\sigma$ ( $\Omega^{-1}\text{m}^{-1}$ )
7200	700	30	0.006	1760	1680	250000	$1.6 \times 10^8$	$7.14 \times 10^5$
$D_s$ (m <sup>2</sup> s <sup>-1</sup> )	$D_L$ (m <sup>2</sup> s <sup>-1</sup> )	$\beta_T$ (K <sup>-1</sup> )	$\beta_C$ (/)					
$1.6 \times 10^{-11}$	$1.0 \times 10^{-8}$	$1.0 \times 10^{-4}$	$4.0 \times 10^{-3}$					

##### 4.3. Boundary conditions

The boundary conditions for the velocity, temperature, turbulent kinetic energy, dissipation rate, species concentration, and current density are set as follows:

*SEN outlet:* Constant values are prescribed for all variables  $u_{inlet,x} = 0$ ,  $u_{inlet,y} = a_b u_{c,y} / d_2$ ,  $k_{inlet} = 1.5(I_t u_{inlet,y})^2$ ,  $\varepsilon_{inlet} = \frac{c_\mu^{0.75} k_{inlet}^{1.5}}{0.07 d_2}$ ,  $T_{inlet} = T_c$ ,  $C_{inlet} = C_c$  and  $\frac{\partial J_y}{\partial y} = 0$ , where  $u_{c,y}$  is the casting velocity in the casting direction, and  $I_t$  is the turbulent intensity calculated from the following relation

$$I_t = 0.16 \text{Re}^{-1/8}, \text{Re} = \rho u_{inlet,y} d_2 / \mu. \quad (26,27)$$

Normal gradient of pressure and current density are set to zero, i.e.  $\frac{\partial P}{\partial y} = 0$  and  $\frac{\partial J_y}{\partial y} = 0$ .

*Billet end:* The pressure outlet is prescribed, where the following boundary conditions are used

$$P = 0, \frac{\partial u_x}{\partial y} = 0, \frac{\partial u_y}{\partial y} = 0, \frac{\partial k}{\partial y} = 0, \frac{\partial \varepsilon}{\partial y} = 0, \frac{\partial T}{\partial y} = 0, \frac{\partial C}{\partial y} = 0, \frac{\partial J_y}{\partial y} = 0. \quad (28)$$

*Top surface (meniscus):* At the meniscus, the symmetry boundary conditions are used (free surface flow). The normal derivative of all variables is set to zero, except the vertical velocity  $u_y$  and the current density  $J_y$  which are set to zero.

*Moving walls:* The walls with the solidified steel move with casting velocity along the casting direction. At the walls, where the liquid phase exists, the no-slip boundary conditions for the velocity are set. In the mould, the Robin boundary condition is used, with the surface heat transfer coefficient equal to 2000 W/(m<sup>2</sup>K). Below the mould, at the secondary cooling system, the heat transfer coefficient is equal to 800 W/(m<sup>2</sup>K). The normal derivative of the solute concentration is set to zero. The current density  $J_x$  is set to zero.

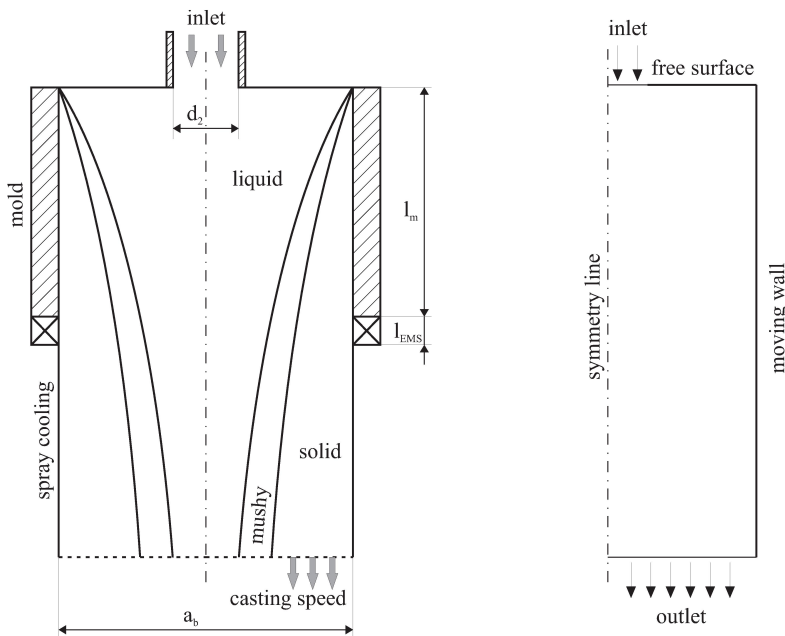


**Figure 1.** Benchmark geometry with typical dimensions.

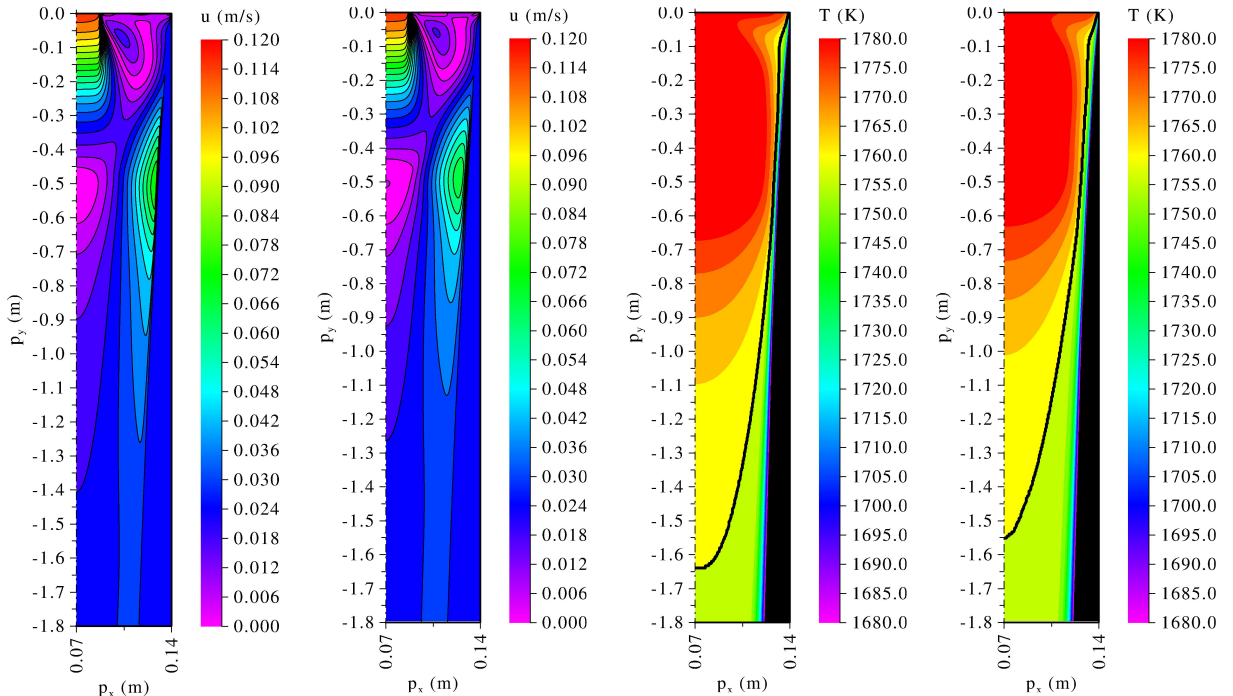
**Figure 2.** Computational geometry.

## 5. Numerical results

In this conference paper, the preliminary numerical results are obtained without electromagnetic forces in momentum equation and with the following simplified microsegregation model

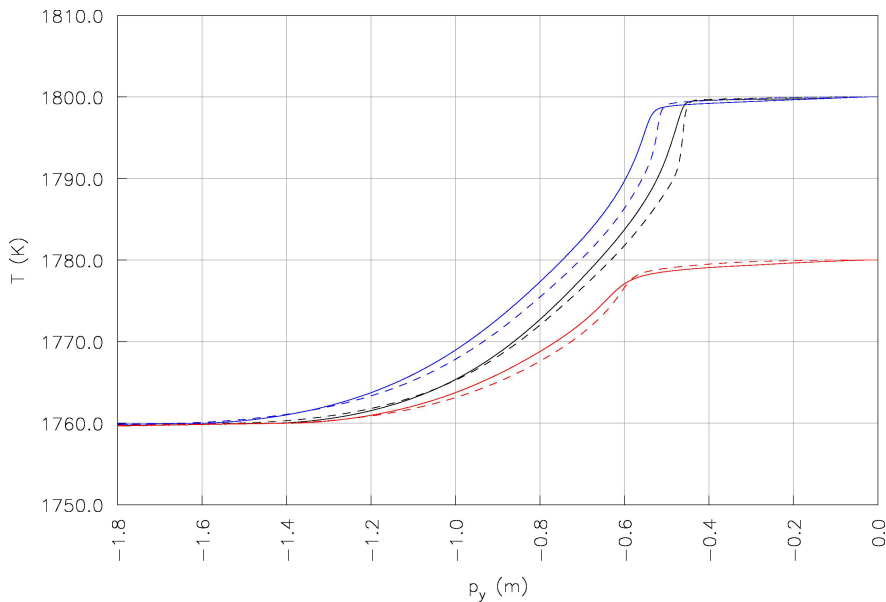
$f_L = (T - T_L) / (T - T_m)$ . Species concentration is assumed to be constant and equal for each phase, i.e.  $C_L = C_C = C$ , which at the present excludes the species transport equation from the solution procedure. The low-Re turbulence model by Abe-Kondoh-Nagano (AKN) [26] is selected, where the normal distance in closure coefficients is calculated up to the wall. The simulation was performed on the node arrangement with 61616 nodes. The steady-state solution shown in figures is approached by a false transient calculation using a fixed time-step of  $10^{-4}$  s. The results are compared with the commercial CFD package Fluent, with the 147408 quadrilateral cells, AKN turbulence model, SIMPLE velocity-pressure coupling, and second-order spatial discretization. The following process parameters were used: reference Case 1:  $u_{cast} = 1.75$  m/min and  $T_{cast} = 1800$  K, enhanced casting speed Case 2:  $u_{cast} = 1.75$  m/min and  $T_{cast} = 1800$  K, and reduced casting temperature Case 3:  $u_{cast} = 1.75$  m/min and  $T_{cast} = 1780$  K.

Figure (3) represents the absolute velocity field in the billet for Case 1. The comparison between LRBFCM and FVM shows very similar flow streaming and re-circulating regions. The temperature field of Case 1 in the range  $T_s \leq T \leq T_{cast}$  is shown in figure (4) with the black line standing for liquidus isotherm. The difference in the position of the liquidus temperature at the symmetry line is about 0.1m, which is expected due to the complex physical phenomena of the modelled process. Figure (5) shows a comparison between centreline temperature for Cases 1-2-3, calculated with FVM and LRBFCM. Figure (6) shows a comparison between surface temperatures for Cases 1-2-3, calculated with FVM and LRBFCM. Figure (7) shows a comparison between horizontal component of the velocity for Cases 1-2-3, calculated with FVM and LRBFCM. Figure (8) shows a comparison between vertical component of the velocity for Cases 1-2-3, calculated with FVM and LRBFCM. The figures (5-8) show excellent agreement between the calculations with both methods and similar response to the change of process parameters, despite different numerical methods used.



**Figure 3.** Absolute velocity field. Left: LRBFCM, right: FVM.

**Figure 4.** Temperature field. Left: LRBFCM, right: FVM. Black line marks liquidus isotherm.



**Figure 5.** Centreline temperatures for Cases 1-2-3. Solid line LRBFCM, dashed line FVM. Case1: black, Case 2: blue, Case 3: red. Casting direction from right to left.

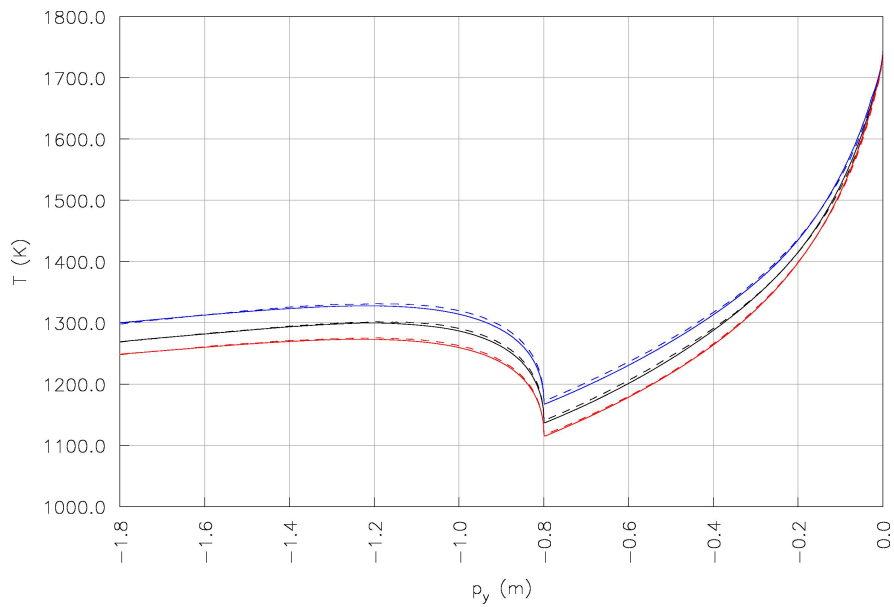


**Figure 6.** Surface temperatures for Cases 1-2-3. Solid line LRBFCM, dashed line FVM. Case1: black, Case 2: blue, Case 3: red. Casting direction from right to left.

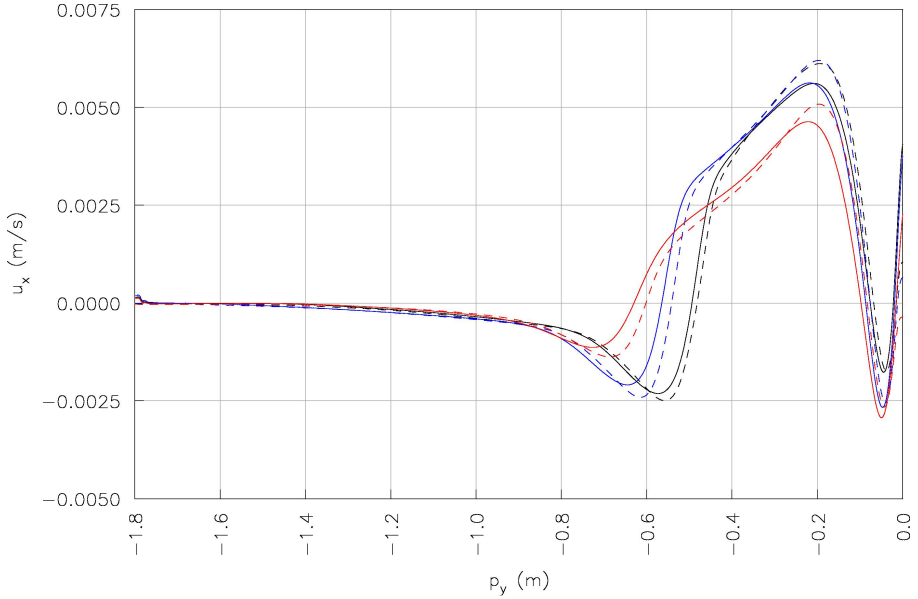


**Figure 7.** Horizontal velocity component  $u_x$  at  $p_x = 0.105$  m for Cases 1-2-3. Solid line LRBFCM, dashed line FVM. Case1: black, Case 2: blue, Case 3: red. Casting direction from right to left.

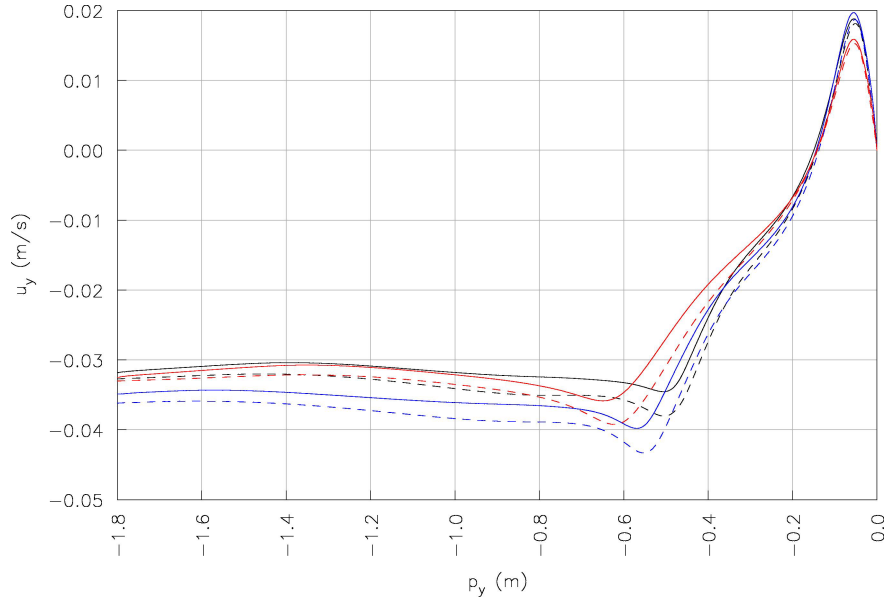


**Figure 8.** Vertical velocity component  $u_y$  at  $p_x = 0.105$  m for Cases 1-2-3. Solid line LRBFCM, dashed line FVM. Case1: black, Case 2: blue, Case 3: red. Casting direction from right to left.

## 6. Conclusions

This paper represents a numerical benchmark proposed for the continuous casting of steel. The geometry and material properties of the continuous casting process are simplified in order to enable straightforward performance comparisons with various numerical methods. In this paper, our in-house developed meshless numerical method, based on the local radial basis function collocation, is used to get the steady state solution of the turbulent fluid flow with heat transfer and solidification. The results

were obtained without electromagnetic forces in the momentum equation and with a simplified microsegregation model with constant and equal concentration of species in each phase. The numerical calculations based on the FVM, were performed with the CFD package Fluent (version 13), and compared with the results obtained by the meshless method. Very good agreement was achieved. The benchmark will be further upgraded and adapted, based on the feedback from the colleges in the field of the numerical modelling of casting processes. A web page of the benchmark results with systematically tabulated results of different numerical methods will be established, similar to [18].

**Acknowledgement:** The comparison exercise is proposed within Slovenian state funded research projects J2-4120, L2-3651 and P2-0379 and co-funded by Štore Steel company. The Centre of Excellence for Biosensors, Instrumentation and Process Control is an operation financed by the European Union, European Regional Development Fund and Republic of Slovenia, Ministry of Higher Education, Science and Technology. The financial support is kindly acknowledged.

## References

- [1] Irwing W R 1993 *Continuous Casting of Steel*, (London: The Institute of Materials)
- [2] Thomas B G 2002 Modeling of the Continuous Casting of Steel - Past, Present Future, [www.brimacombe.org/pdf/2001\\_Thomas.pdf](http://www.brimacombe.org/pdf/2001_Thomas.pdf)
- [3] Zhao B, Thomas B G, Vanka S P and O'Malley R J 2005 *Metall. Mater. Trans. B* **36** 801-23
- [4] Reza Aboutalebi M, Hasan M and Guthrie R I L 1993 *Metall. Mater. Trans. B* **26** 731-44
- [5] Kim D S, Kim W S and Cho K H 2000 *ISIJ Int.* **40** 670-76
- [6] Kang K G, Ryou H S and Hur N K 2005 *Numer. Heat Tr. A* **48** 461-81
- [7] Kubo N, Ishi T, Kubota J and Ikagawa T 2004 *ISIJ Int.* **44** 556-64
- [8] Moon C H and Hwang S M 2003 *Int. J. Numer. Meth. Eng.* **57** 315-39
- [9] Vertnik R, Založnik M and Šarler B 2006 *Eng. Anal. Bound. Elem.* **30** 847-55
- [10] Vertnik R, Šarler B and Senčič B 2009 Simulation of turbulent flow and heat transfer in continuous casting of billets by a meshless method. *3rd International Conference on Simulation and Modelling of Metallurgical Processes in Steelmaking-STEELSIM2009* (Leoben, Austria, 8-10 September 2009) ed A Ludwig (Leoben, Austria: ASMET) pp 155-61
- [11] Vertnik R 2010 *Heat and fluid flow simulation of the continuous casting of steel by a meshless method-dissertation* (Nova Gorica, SLO: University of Nova Gorica, XVII) p 225, <http://www.p-ng.si/~vanesa/doktorati/karakterizacija/8Vertnik.pdf>
- [12] Chaudhary R, Ji C, Vanka S P, and Thomas B G 2011 *Metall. Mater. Trans. B* **42** 987-1007
- [13] Šarler B and Vertnik R 2006 *Comput. Math. Appl.* **51** 1269-82
- [14] Vertnik R and Šarler B 2006 *Int. J. Numer. Method H.* **16** 617-640
- [15] Kosec G and Šarler B 2009 *Int. J. Numer. Method H.* **18** 868-82
- [16] Kosec G and Šarler B 2009 *Comput. Model. Eng. Sci.* **47** 191-216
- [17] Gobin D and Le Quéré P 2000 *Comput. Assist. Mech. Eng. Sci.* **7** 289-306
- [18] Bellet M, Combeau H, Fautrelle Y, Gobin D, Rady M, Arquis E, Budenkova O, Dussoubs B, Duterrail Y, Kumar A, Gandin C A, Goyeau B, Mosbah S and Založnik M 2009 *Int. J. Therm. Sci.* **48** 2013-16
- [19] Kosec G, Založnik M, Šarler B and Combeau H 2011 *Comput. Mater. Con.* **22** 169-59
- [20] Šarler B, Vernik R, Šaletić S and Cesar J 2005 *Berg-Huettenmaenn. Monatsh.* **150** 300-6
- [21] Chorin A J 1967 *J. Comput. Phys.* **2** 12-26
- [22] Bennion W D and Incropera F P 1988 *Numer. Heat Tr. A-Appl.* **13** 277-96
- [23] Wilcox, D C 1993 *Turbulence modeling for CFD* (California: DCW Industries, Inc.)
- [24] Vertnik R and Šarler B 2009 *Comput. Model. Eng. Sci.* **44** 66-95
- [25] Buhmann M D 2003 *Radial Basis Function: Theory and Implementations* (Cambridge: Cambridge University Press)
- [26] Abe K, Kondoh T and Nagano Y 1994 *Int. J. Heat Mass Tran.* **37** 139-51